Materials Transactions, Vol. 49, No. 5 (2008) pp. 1084 to 1088
Special Issue on Platform Science and Technology for Advanced Magnesium Alloys, IV

Effect of Ca and CaO on the High Temperature Oxidation of AZ91D Mg Alloys

Dong-Bok Lee, Lee-Seok Hong* and Young-Jig Kim

School of Advanced Materials Science & Engineering, Sungkyunkwan University, Suwon 440-746, Korea

Magnesium alloys of AZ91D, AZ91D + (1, 3, 5) mass% Ca, and AZ91D + (0.5, 1) mass% CaO were cast and oxidized at high temperature in atmospheric air in order to study the effect of Ca and CaO on the oxidation. The microstructure of the CaO-added alloys was similar to that of the Ca-added alloys. Ca and CaO both formed Al_2Ca in the alloys, but Ca was more effective than CaO in increasing the oxidation resistance of Mg alloys. The microstructure and composition of the scale formed on the CaO-added alloys were similar with those on the Ca-added alloys. [doi:10.2320/matertrans.MC200799]

(Received October 5, 2007; Accepted December 17, 2007; Published February 6, 2008)

Keywords: *magnesium, calcium, calcium oxide, oxidation*

1. Introduction

The use of magnesium alloys as light-weight structural materials is increasing due to their excellent properties such as high specific strength, high specific rigidity, and the lowest density among metallic materials in practical use. However, the widespread usage of magnesium alloys is limited due to their poor oxidation resistance. Magnesium oxidizes relatively slowly below 673 K owing to the formation of a protective MgO scale. However, magnesium begins to oxidize rapidly above 723 K, and ignition starts above 773 K simultaneously in localized regions before spreading over the entire surface.[1)] Magnesium evaporates easily owing to its relatively high vapor pressure. In a previous study, in order to suppress the vigorous reaction of molten Mg with oxygen during melting, a small amount of Ca was added.[2)] Ca is thought to be a good candidate for suppressing oxidation as it has a lower density than either Mg or Al and has a very high affinity for oxygen. There is also evidence that adding a small amount of Ca improves high-temperature properties, such as creep.[3)] The formation of a thin CaO-rich outer layer on the surface has been shown to effectively retard oxidation and ignition of Mg alloy ingots.[4,5)] In these studies, the inner layer was either a mixture of (MgO, CaO) in the case of Mg + (0.5~3) mass% Ca alloys,[4)] or a mixture of (MgO, CaO, Al_2O_3) in the case of AZ91 + (0.3~5) mass% Ca alloys.[5)] AZ91D is the Al-rich, high-strength cast Mg alloy that is most widely used.

In a preliminary study we found that CaO particles were also effective in suppressing rapid oxidation and burning of the molten Mg alloy. The reason for this beneficial effect has not yet been adequately investigated. Also, the effect of CaO on the oxidation of the AZ91D ingot still needs to be investigated, as the stable CaO particles were expected to serve as reinforcing ceramics in the metal matrix. Furthermore, the use of low-cost CaO is desirable for industrial applications. This study has the following three important points: (1) AZ91 alloys containing CaO particles were cast, and subsequently oxidized in order to determine their microstructure and oxidation behavior. (2) Pt marker tests were performed on AZ91 + Ca and AZ91 + CaO alloys to understand the oxidation mechanism during thin scale formation. (3) Systematic analyses on the oxidized alloys were done utilizing transmission electron microscopy (TEM). This study aims to elucidate the effect of Ca and CaO on the high temperature oxidation characteristics of AZ91D alloys. The alloy microstructure, the oxide scales formed, and the oxidation mechanism are also examined.

*Graduate Student, Sungkyunkwan University

2. Experimental Procedure

Commercially available AZ91D alloys (Al = 8.8, Zn = 0.7, Mn = 0.22 in mass%, Mg = balance) were melted in steel crucibles in an electric resistance furnace under a CO_2 + 1% SF_6 protective atmosphere. The melt was rotated for uniform mixing at 953 K using a stirrer positioned at the top of the crucible, and Ca chips (98.5% pure) or CaO particles (98.5% pure, 38~100 μm in size) were added at a feed rate of 0.17 g/s under a rotational speed of 13 rev./s.[6)] The five kinds of Mg alloys prepared were AZ91D + (1, 3, 5) mass% Ca and AZ91D + (0.5, 1) mass% CaO. Since CaO decreased the fluidity of the alloy melt, the amount added was limited to 1 mass%. The alloy samples were cut into 12 mmφ × 10 mm coupons, ground to a 1000 grit finish, degreased, and oxidized in atmospheric air. Ignition tests were performed by inserting a thermocouple into a hole drilled in the center of the sample. The samples were inspected by a scanning electron microscope (SEM) equipped with an energy dispersive spectrometer (EDS), X-ray photoelectron spectroscope (XPS), Auger electron spectroscope (AES), X-ray diffractometer (XRD with Cu-K_α radiation), and TEM equipped with an EDS (0.5 nmφ spot size). The TEM sample was prepared by milling, using a focused-ion-beam (FIB) system with a liquid-gallium-metal ion source and a maximum accelerating voltage of 30 kV.

3. Results and Discussion

Figure 1(a) shows the XRD pattern of AZ91D after oxidation at 673 K for 360 ks. The matrix consisted primarily of α-Mg as the major phase and $Al_{12}Mg_{17}$ as the minor phase. Under equilibrium conditions, the Mg-9%Al melt solidifies

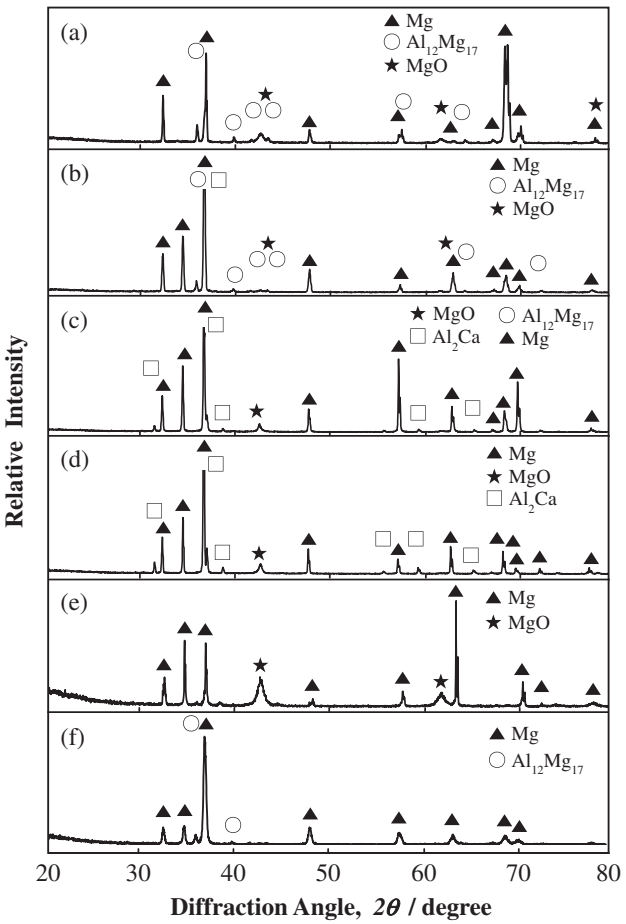

Fig. 1 XRD patterns taken after oxidation. (a) AZ91D (673 K/360 ks), (b) AZ91D + 1% Ca (673 K/360 ks), (c) AZ91D + 3% Ca (673 K/360 ks), (d) AZ91D + 5% Ca (673 K/360 ks), (e) AZ91D + 5% Ca (723 K/180 ks), (f) AZ91D + 1% CaO (623 K/180 ks).

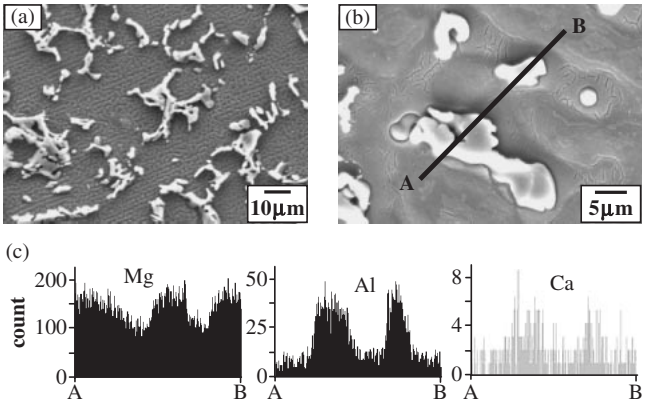

Fig. 2 (a) Etched SEM microstructure of AZ91D + 3% Ca, (b) etched SEM microstructure of AZ91D + 0.5% CaO, (c) EDS line profiles along A-B of (b).

into Mg(s) and $Al_{12}Mg_{17}$(s) by the eutectic reaction.[7] MgO peaks were weak owing to the fact that the scale formed was very thin. Figure 1(b) shows the XRD pattern of AZ91D + 1% Ca after oxidation at 673 K for 360 ks, where the matrix phases were the same as above. The MgO scale that formed was hardly visible, owing to increased oxidation resistance. Figure 1(c) shows the XRD pattern of AZ91D + 3% Ca after oxidation at 673 K for 360 ks. In this case, the Ca added formed insoluble Al_2Ca, and as the amount of Al_2Ca increased, the amount of $Al_{12}Mg_{17}$ decreased. There was also a faint indication of MgO. Figure 1(d) shows the XRD pattern of AZ91D + 5% Ca after oxidation at 673 K for 360 ks. $Al_{12}Mg_{17}$ was not detected, but Al_2Ca was, while MgO was the only oxide detected. Figure 1(e) shows the XRD pattern of AZ91D + 5% Ca after oxidation at 723 K for 180 ks. Owing to the thickened MgO scale, only α-Mg was detected as the matrix. Figure 1(f) shows the XRD pattern of AZ91D + 1% CaO after oxidation at 623 K for 180 ks. The matrix consisted primarily of α-Mg as the major phase and $Al_{12}Mg_{17}$ as the minor phase. In the case of the AZ91D + 10% CaO alloy that we have cast separately, only α-Mg and Al_2Ca were detected as the matrix phases. No oxides were detected in Fig. 1(f) because of the thin scale formation. On the other hand, at the later stage of oxidation, thick, porous oxide scales that consisted primarily of MgO formed. The scale formed on AZ91D consisted of randomly oriented MgO with traces of $MgAl_2O_4$ spinel.[1]

Figure 2(a) shows a typical microstructure of AZ91D + Ca alloys. The primary α-Mg grains that were a solid solution of Al and Zn in Mg[8] were surrounded by the secondary phases interconnected along grain boundaries. The secondary phases were either $Al_{12}Mg_{17}$[9] or Al_2Ca. Figures 2(b) and (c) show a typical microstructure and the corresponding EDS line profiles of AZ91D + CaO alloys, respectively. The CaO particles that were initially added were gone; instead, Al_2Ca particles were seen over the α-Mg matrix. At the casting temperature of 953 K, the standard free energy change, ΔG^o, of reaction of Mg(l) + 2 Al(l) + CaO(s) = Al_2Ca(s) + MgO(s) was −169 kJ, indicating that the forward reaction could occur spontaneously. Since the MgO formed was denser than the melt, MgO impurities sank to the bottom of the melt. Also, some oxygen released from CaO floated toward the surface, forming MgO impurities at the top of the melt. Nevertheless, CaO, like Ca, suppressed ignition of the melt and thereby diminished the usage of environmentally hazardous SF_6 gas during melting.

At higher temperatures, oxidation rates increased sharply, and a fracture of the oxide occurred, leading to the ignition of alloys. The ignition temperatures determined from Fig. 3 increased to 781 K (AZ91D), 813 K (AZ91D + 0.5% CaO), 871 K (AZ91D + 1% CaO), 1007 K (AZ91D + 1% Ca), 1049 K (AZ91D + 3% Ca), and 1365 K (AZ91D + 5% Ca). Clearly, higher CaO or Ca content results in better oxidation resistance of Mg alloys. Ca was more effective than CaO in improving resistance, which was reasonable considering the dissociation of CaO during melting. The ignition temperature of the AZ91 alloy reported elsewhere was 858 K.[10] This difference in temperature is attributed to the fact that ignition strongly depends on the heating rate, alloy chemistry, and specimen geometry because high specific area promotes ignition.

Figures 4(a) and (b) show the XPS spectra of AZ91D + 5% Ca and AZ91D + 1% CaO after oxidation at 773 K for 46.8 ks, respectively. For both alloys, the surface scale consisted of CaO (E_b of $Ca_{2p3/2}$ = 347.3~347.4 eV) and

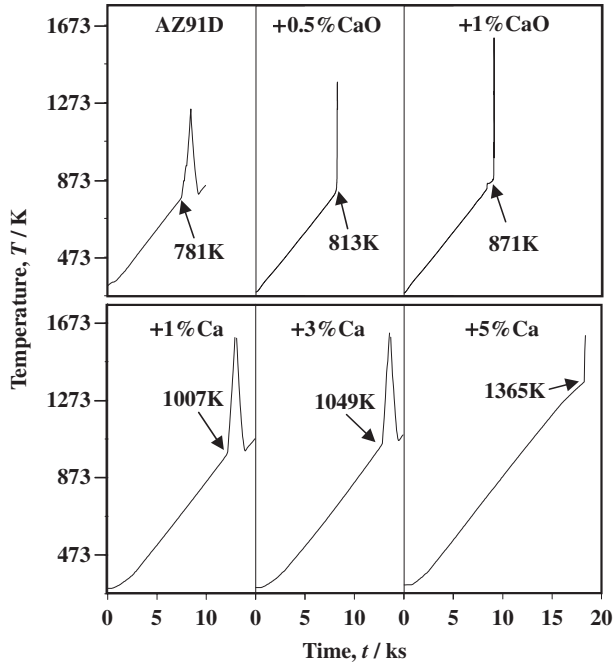

Fig. 3 Ignition test graphs of AZ91D + (0, 1, 3, 5)% Ca, and AZ91D + (0.5, 1)% CaO. Heating rate = 66.7 K/ks in air.

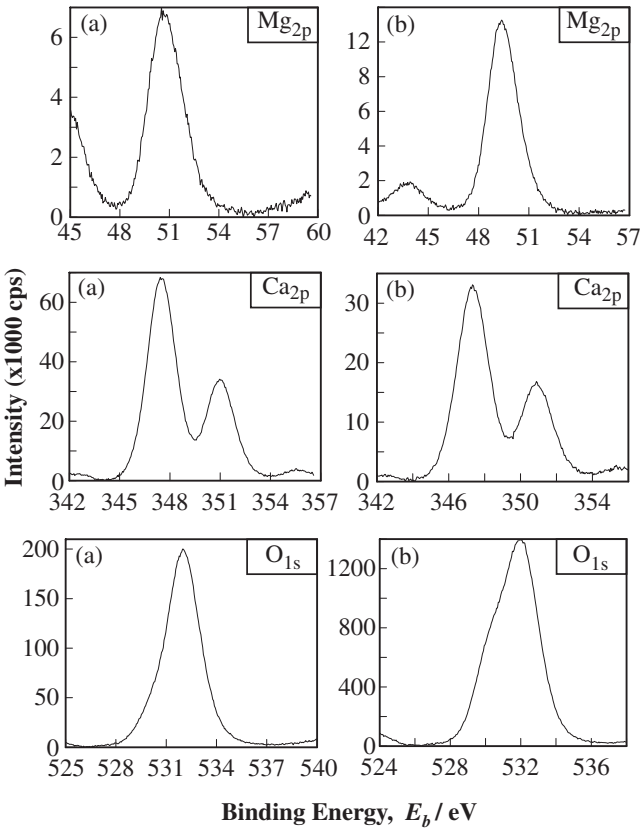

Fig. 4 XPS spectra of Mg_{2p}, Ca_{2p} and O_{1s} taken from the outermost surface scale formed after oxidation at 773 K for 46.8 ks in air. (a) AZ91D + 5% Ca, (b) AZ91D + 1% CaO.

MgO (E_b of Mg_{2p} = 50.5, 49.3 eV). In the case of pure CaO and MgO, measured values were E_b of $Ca_{2p3/2}$ = 346.5 eV and E_b of Mg_{2p} = 50.1 eV, respectively. This shift in maximum binding energy of Ca_{2p} and Mg_{2p} may be due to

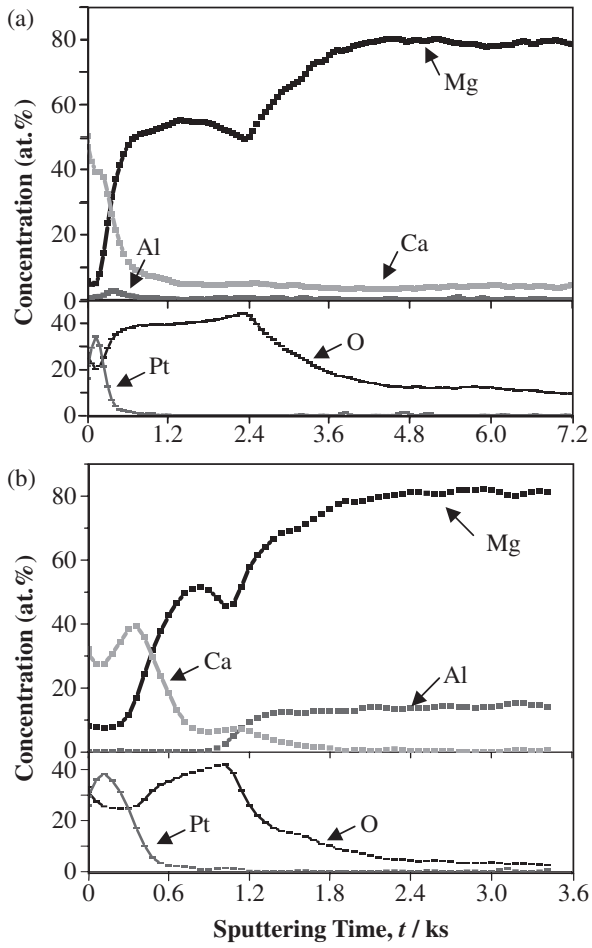

Fig. 5 AES depth profiles taken after oxidation at 723 K for 144 ks in air. The penetration rate is 330 nm/ks for the reference SiO_2. (a) AZ91D + 5% Ca, (b) AZ91D + 1% CaO.

the presence or doping of minor elements in the surface scale. It is noted that the EPMA analyses indicated that Zn was incorporated throughout the scale as the minor element. On the other hand, CaO and MgO both exist in the rocksalt structure. Mixing these compounds at high temperatures is therefore expected to lead to a substitutional arrangement of Ca and Mg ions on the cationic sublattice.[11] However, such substitution may not occur in this study, because CaO and MgO are virtually immiscible over the current test temperature range. The asymmetric, broad O_{1s} spectrum peak (E_b = 531.9 eV) indicates that more than one oxygen-containing species was involved. Most of the oxygen present was in the form of CaO and MgO.

Figures 5(a) and (b) show AES depth profiles of AZ91D + 5% Ca and AZ91D + 1% CaO taken after oxidation at 723 K for 144 ks, respectively. These alloys were oxidation-resistant under the current conditions. To understand the oxidation mechanism, a thin Pt film was deposited on top of the specimen prior to oxidation. From the location of the Pt marker, it can be seen that the outermost surface scale formed by reaction of oxygen with the outwardly diffused Mg and Ca ions. The inner oxide layer was formed primarily by a reaction with oxygen that transported into the material. The consumption of Ca in the outermost surface scale resulted in the strong depletion of Ca in the inner oxide layer. Both CaO

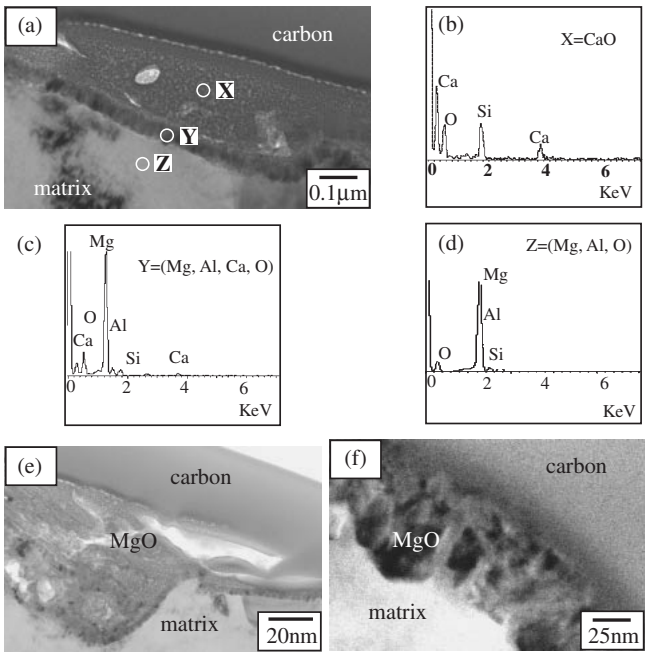

Fig. 6 TEM/EDS analyses on AZ91D + 5% Ca after oxidation at 673 K for 180 ks. (a) image of CaO grain, (b) spectrum of 'X', (c) spectrum of 'Y', (d) spectrum of 'Z', (e) image of MgO grain, (f) image of an array of fine MgO grains.

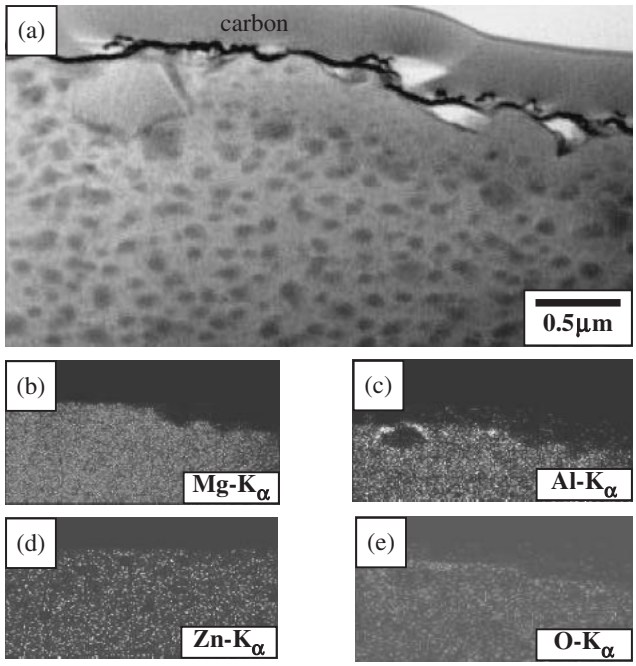

Fig. 7 AZ91D + 1% CaO after oxidation at 673 K for 180 ks. (a) cross-sectional TEM image, and EDS mappings of (b) Mg, (c) Al, (d) Zn and (e) oxygen.

and MgO have Schottky defects, and cations diffuse faster than oxygen.[12–14] Hence, one can expect that the oxide scale would primarily form by the outward diffusion of Mg and Ca under normal conditions. In reality, since the Pilling-Bedworth ratios of MgO and CaO were 0.81 and 0.64, respectively,[15] these oxides could not form a compact layer and systematic fissuring occurred as oxidation progressed. In the later stages of oxidation, the loose oxide layer allowed oxygen to penetrate and acted as a channel for the transport of Mg vapor. Nevertheless, when the scale was thin, scale formation occurred by the inwardly transported oxygen, as shown in Fig. 5. Abundant Ca and some Mg were present in the outermost surface scale in Fig. 5. Ca was the most active and diffused rather easily toward the surface. Mg diffused faster than Ca in CaO, although both their diffusion rates were relatively slow.[13] Hence, the formation of CaO cannot prevent formation of MgO in the outermost surface scale. Al is the most noble among Mg, Al and Ca. Hence, Al oxidized either to a small amount in the bottom part of the outermost surface scale (Fig. 5(a)) or roughly *in situ* in the inner oxide layer (Fig. 5(b)). Regardless of its location, Al was oxidized primarily by the inwardly transported oxygen (Fig. 5). Since the added CaO particles were dissolved off during melting, both the Ca-added and CaO-added alloys behaved similarly according to Fig. 5.

Figure 6 shows TEM images and the corresponding EDS spectra of the oxide scale formed on AZ91D + 5% Ca after oxidation at 673 K for 180 ks. Figure 6(a) shows a CaO grain, as confirmed from Fig. 6(b). Here, the Si signal is spurious and arises from the support used for the thin foil specimen. The scale/matrix interface (*i.e.*, point Y) consisted of Mg, Al, Ca and 25% oxygen (Fig. 6(c)), while the matrix below the scale consisted of Mg, Al and 5% oxygen (Fig. 6(d)). The subscale region inevitably had dissolved oxygen that penetrated beyond the oxide scale.

Figure 6(e) shows a MgO oxide grain, which EDS analyses revealed was impure. Depending on the location, (1∼8)% Ca and (0∼11)% Al were heterogeneously distributed within the MgO grain. Figure 6(f) shows an array of nanometer-size, round MgO grains. These had (0∼1)% Ca and (0∼1)% Al. Below the MgO layer, oxygen dissolution was confirmed by EDS. Since CaO has a lower vapor pressure than MgO, and cation diffusion in CaO was slower than that in MgO,[16] the oxidation resistance of AZ91D increased with the addition of Ca. However, this beneficial effect was not substantial because CaO was inherently a non-protective oxide (Pilling-Bedworth ratio = 0.64). Hence, all the alloys tested were prone to severe oxidation or even burning at high temperatures. For example, during the isothermal oxidation at 723 K in air, the time for ignition was approximately 90 ks for AZ91D, 180 ks for AZ91D + (0.5, 1)% CaO, 180 ks for AZ91D + 1% Ca, 216 ks for AZ91D + 3% Ca, and 324 ks for AZ91D + 5% Ca. Since the dissociation of CaO provided the alloy with oxygen, CaO only slightly increased the oxidation resistance of Mg alloys. Previously, it has been argued that Ca enhanced the formation of a thin and uniform oxide layer and prevented the growth of thick nodular oxides.[17] However, a more accurate explanation may be as follows: The role of Ca is to retard the oxidation of Mg alloys through the formation of CaO having low vapor pressure and high stoichiometry. Ca cannot prevent, but can simply delay the growth of thick nodular oxides, because CaO is a non-protective oxide. The initially formed thin MgO oxide layers with and without CaO-addition were therefore inevitably destroyed at high temperatures.

Figure 7(a) shows the TEM image of AZ91D + 1% CaO after oxidation at 673 K for 180 ks. The oxygen content was about 10% according to the EDS analysis. Figures 7(b)–(e) indicate that the alloy shown was not yet oxidized. Hence, it is proposed that the oxidation of the alloy proceeds via not only the oxide formation but also oxygen dissolution from the surface. The thin oxide layers shown in Figs. 6 and 7 later became thick. Also, oxide nodules developed into a cauliflower-like morphology and ignition started. Such behavior could also be observed in many Mg alloys. The breakage of thickly grown oxide scales allows the easy penetration of oxygen beyond the oxide scales, resulting in the vigorous reaction of oxygen with the underlying Mg alloys that have dissolved oxygen.

4. Conclusions

The microstructure and oxidation behavior of AZ91D + CaO alloys were basically the same as those of AZ91D + Ca alloys. Ca and CaO formed Al_2Ca in the matrix. CaO was less effective than Ca, mainly due to its dissociation during casting. CaO suppressed ignition of the melt and thereby diminished the usage of SF_6 gas during casting, as Ca did. The higher the concentration of Ca and CaO, the better the oxidation resistance was. During the early stage of oxidation, Mg and Ca ions diffused outward to form the outermost scale. At the same time, oxygen diffused inward to form the inner oxide layer consisting of polycrystalline CaO and MgO. Oxygen was also observed to dissolve in the subscale. During the later stage of oxidation, rapid oxidation and ignition occurred.

Acknowledgements

This work was supported by Samsung Research Fund, Sungkyunkwan University, 2007.

REFERENCES

1) F. Czerwinski: Acta Mater. **50** (2002) 2639–2654.
2) M. Sakamoto, S. Akiyama and K. Ogi: J. Mater. Sci. Lett. **16** (1997) 1048–1050.
3) C. Mendis, L. Bourgeois, B. Muddle and J. F. Nie: *Magnesium Technology 2003*, ed. by H. I. Kaplan, (TMS, Warrendale, PA, 2003), pp. 183–188.
4) B. S. You, W. W. Park and I. S. Chung: Scripta Mater. **42** (2000) 1089–1094.
5) B. H. Choi, B. S. You, W. W. Park, Y. B. Huang and I. M. Park: Met. Mater., Int. **9** (2003) 395–398.
6) S. K. Kim and Y. J. Kim: Mater. Sci. Technol. **16** (2000) 1–5.
7) T. B. Massalski: *Binary Alloy Phase Diagrams*, vol. 1 (ASM, Metals Park, OH, 1986) p. 129.
8) F. Czerwinski: Corros. Sci. **46** (2004) 377–386.
9) J. Chen, J. Wang, E. Han, J. Dong and W. Ke: Mater. Corros. **57** (2005) 789–793.
10) N. V. Ravi Kumer, J. J. Blandin, M. Suery and E. Grosjean: Scripta Mater. **49** (2003) 225–230.
11) G. Ceder, P. D. Tepesch, A. F. Kohan and A. Van Der Ven: J. Electroceramics **1** (1977) 15–26.
12) B. J. Wuensch, W. C. Steele and T. Vasilos: J. Chem. Phys. **58** (1973) 5258–5266.
13) D. K. Fisler and R. T. Cygan: Am. Mineralogist **84** (1999) 1392–1399.
14) J. H. Park and T. F. Kassner: J. Nucl. Mater. **233–237** (1996) 476–481.
15) D. A. Jones: *Principles and Prevention of Corrosion*, 2nd ed. (Prentice Hall, NJ, 1996) p. 419.
16) S. Mrowec: *Defects and Diffusion in Solids*, (Elsevier Pub. Co., New York, 1980) p. 432.
17) B. H. Choi, I. M. Park, B. S. You and W. W. Park: Mater. Sci. Forum, **419–422** (2003) 639–644.